



# Postmodulation of the Metal–Organic Framework Precursor toward the Vacancy-Rich Cu<sub>x</sub>O Transducer for Sensitivity Boost: Synthesis, Catalysis, and H<sub>2</sub>O<sub>2</sub> Sensing

Serge Cosnier, Junji Li, Wen-Li Xin, Yu-Xuan Dai, Guofang Shu, Xue-Ji Zhang, Robert Marks, Dan Shan

## ► To cite this version:

Serge Cosnier, Junji Li, Wen-Li Xin, Yu-Xuan Dai, Guofang Shu, et al.. Postmodulation of the Metal–Organic Framework Precursor toward the Vacancy-Rich Cu<sub>x</sub>O Transducer for Sensitivity Boost: Synthesis, Catalysis, and H<sub>2</sub>O<sub>2</sub> Sensing. *Analytical Chemistry*, 2021, 93 (32), pp.11066-11071. 10.1021/acs.analchem.1c02183 . hal-03376495

**HAL Id: hal-03376495**

**<https://hal.science/hal-03376495>**

Submitted on 13 Oct 2021

**HAL** is a multi-disciplinary open access archive for the deposit and dissemination of scientific research documents, whether they are published or not. The documents may come from teaching and research institutions in France or abroad, or from public or private research centers.

L'archive ouverte pluridisciplinaire **HAL**, est destinée au dépôt et à la diffusion de documents scientifiques de niveau recherche, publiés ou non, émanant des établissements d'enseignement et de recherche français ou étrangers, des laboratoires publics ou privés.

This document is confidential and is proprietary to the American Chemical Society and its authors. Do not copy or disclose without written permission. If you have received this item in error, notify the sender and delete all copies.

**Modulation of Crystalline Metal-organic Framework  
Precursor towards Carbon-based CuxO Electro-catalyst for  
Boosting Sensitive Hydrogen Peroxide Detection: Synthesis,  
Catalysis and Sensing Application**

Journal:	<i>Analytical Chemistry</i>
Manuscript ID	ac-2021-021836
Manuscript Type:	Technical Note
Date Submitted by the Author:	24-May-2021
Complete List of Authors:	Li, Junji; Nanjing University of Science and Technology, School of Environmental & Biological Engineering Xin, Wen-Li; Nanjing University of Science and Technology Dai, Yu-Xuan; Nanjing University of Science and Technology, School of Environmental & Biological Engineering Shu, Guofang; Southeast University Zhongda Hospital Zhang, Xueji; Nanjing University of Science and Technology, School of Environmental & Biological Engineering Marks, Robert; Ben-Gurion University of the Negev, Department of Biotechnology Engineering Cosnier, Serge; Universite Grenoble Alpes, Département de Chimie Moléculaire UMR CNRS 5250 Shan, Dan; Nanjing University of Science and Technology, School of Environmental and Biological Engineering

SCHOLARONE™  
Manuscripts

**Modulation of Crystalline Metal-organic Framework  
Precursor towards Carbon-based Cu<sub>x</sub>O Electro-catalyst for  
Boosting Sensitive Hydrogen Peroxide Detection: Synthesis,  
Catalysis and Sensing Application**

Junji Li<sup>a</sup>, Wen-Li Xin<sup>a</sup>, Yu-Xuan Dai<sup>a</sup>, Guofang Shu<sup>b</sup>, Xue-Ji Zhang<sup>a</sup>, Robert S. Marks<sup>c</sup>,  
Serge Cosnier<sup>d</sup>, Dan Shan<sup>a\*</sup>

<sup>a</sup> School of Environmental and Biological Engineering, Nanjing University of Science and  
Technology, Nanjing 210094, China

<sup>b</sup> Department of Clinical Laboratory, Zhongda Hospital, Southeast University School of  
Medicine, Nanjing, 210009, Jiangsu, China

<sup>c</sup> Department of Biotechnology Engineering, Ben-Gurion University of the Negev, Beer-Sheva,  
Israel

<sup>d</sup> University of Grenoble Alpes-CNRS, DCM UMR 5250, F-38000 Grenoble, France

**\* Corresponding to:**

**Prof. Dan Shan**

School of Environmental and Biological Engineering,

Nanjing University of Science and Technology,

Nanjing, Jiangsu, 210094, China.

Tel. +86(25) 84303107;

E-mail: danshan@njust.edu.cn

**Abstract:**

Metal-organic frameworks (MOFs) act as versatile coordinators for the subsequent synthesis of high-performance electrochemical catalysts by providing dispersed metal-ion distribution, initial coordination condition, and modular dopant atom ratios, etc. In this work, a copper-based crystalline MOF *trans*-[Cu(NO<sub>3</sub>)<sub>2</sub>(Him)<sub>4</sub>] was synthesized as a novel precursor of a carbon-based electrochemical valence-alternating NC@Cu<sub>x</sub>O catalyst. Through simple temperature modulation of the pyrolysis procedure, the gradual transformation towards highly-active catalytic nanocomposite was characterized and investigated to ascertain the signal enhancing mechanism during H<sub>2</sub>O<sub>2</sub> detection. Owing to its proprietary structure and ensuing electrochemical reduction activity, a proof-of-principle sensor using NC@Cu<sub>x</sub>O as transducer was able to provide an amplified sensitivity of 2330 μA mM<sup>-1</sup> cm<sup>-2</sup>. In addition, its facile one-vessel preparation and the intrinsic non-enzymatic nature suggests a wide range of potential applications in medical settings.

**Keywords:**

Metal-organic framework derivate, Non-enzyme catalyst, Electrochemical biosensor, Fenton-like signal amplification, One-pot synthesis

1  
2  
3  
4 47 The electrochemically active material, or rather the transducer, plays an  
5  
6 48 imperative role in the construction of an electrochemical biosensor <sup>1</sup>. Its  
7  
8  
9 49 intrinsic properties, such as active center density, electron transfer ability, as  
10  
11  
12 50 well as, internal structure and external morphology, set the fundamental  
13  
14  
15 51 performance of the derived sensing systems or devices <sup>2-4</sup>. Use of  
16  
17 52 metal-organic frameworks (MOFs) as self-sacrificed precursors <sup>5, 6</sup> provides  
18  
19  
20 53 invaluable properties, such as: 1) tunable initial coordination environment and  
21  
22  
23 54 heteroatom doping, that can be easily achieved through the selection of  
24  
25  
26 55 multitudinous ligand molecules; 2) atomic migration process can be accessed  
27  
28  
29 56 and manually paused to obtain a series of products with diverse composite  
30  
31  
32 57 configurations, including metal centers at different valence states or more  
33  
34  
35 58 precisely the nuanced electronic regulation states, or carbon substrates with  
36  
37  
38 59 various interconnecting degrees or doping ratios, and active catalysis clusters  
39  
40  
41 60 with distinguished diameters; 3) porous characteristics can be inherited, thus  
42  
43  
44 61 allowing high-throughput mass diffusion and interfacial contact <sup>7, 8</sup>. Already,  
45  
46  
47 62 some state-of-the-art single atom catalysts (SACs) with satisfactory  
48  
49  
50 63 performance have been synthesized using MOFs as starting templates <sup>9, 10</sup>.

51  
52  
53 64 Copper-based MOFs or derived nanomaterials have drawn conspicuous  
54  
55  
56 65 attention due to their specific enzyme-like activities, reasonable cost efficiency  
57  
58  
59 66 and robust stability <sup>11-13</sup>. According to the aforementioned advantages, these  
60  
61  
62 67 copper-based enzyme mimics have been well accepted as signal transducers  
63  
64  
65 68 to construct sensitive biosensor systems <sup>14</sup>. Copper species, no matter in  
66

forms of elementary clusters <sup>15, 16</sup>, compound nanoparticles <sup>17</sup> or even secondary coordination units <sup>18</sup>, show prominent redox activity, with or without, extra potential energy from the external circuit. In some latest articles, more complex copper-based transducer materials with excellent and versatile capabilities were synthesized from MOFs-contained composite precursors, e.g. with several 2D materials like graphene, C<sub>3</sub>N<sub>4</sub> or MXene <sup>19</sup>. All these treasures figure out an efficient clue of massively converting homogeneous structural units inside the MOF crystal into highly disperse nano-catalysts decorated upon a simultaneously generated substrate, and meanwhile investigate the transiting procedure of some certain catalysis activity to the other <sup>20</sup>.

In the present communication, we designed the synthesis of a crystalline MOF-derived Cu<sub>x</sub>O composite catalyst, serving as an electrochemical peroxidase mimic. Inspired by the coordination structure of copper catalysts, both the ligand atoms and the central metal valence state of the catalysis unit were modulated simply using a short period of differential thermal treatment. Thanks to the uniform texture of the crystalline precursor, the generation process of a well-tuned transducer material was monitored and sought. An electrochemical Fenton-like signal enhancing mechanism was herein discussed, in view of the derived prototype biosensor and its corresponding interfacial reactions (Fig. 1A). We expect that this novel and concise transducer material will provide proprietary engineering insights in providing

improved biosensor devices suitable for commercialization<sup>21, 22</sup>.

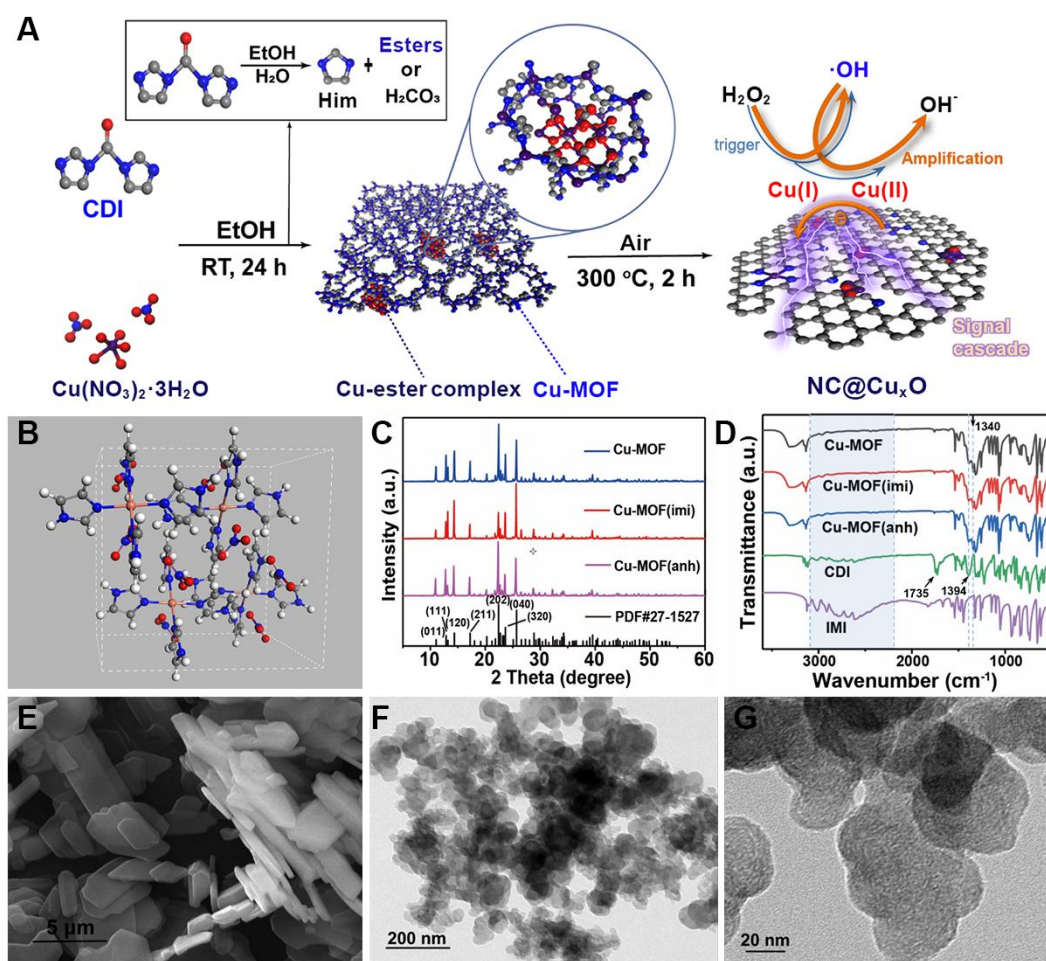
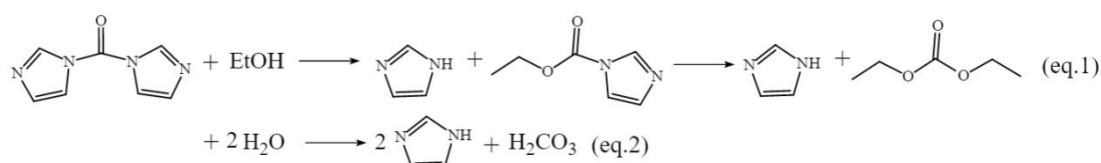


**Fig. 1.** Stepwise modulation from crystalline MOF precursor to active electrochemical transducer. (A) Schematic overview of the preparation and signal amplification mechanism of the composite transducer material NC@Cu<sub>x</sub>O. (B) Crystal structure diagram of the MOF precursor *trans*-[Cu(NO<sub>3</sub>)<sub>2</sub>(Him)<sub>4</sub>]. (C) Three comparative routes to prepare MOF precursors with distinguished preferential crystallographic orientation and lattice shrinkage or bulge. (D) FT-IR spectra of the obtained crystalline precursors with arrows and blue dashed lines or region indicating critical changes of the transmittance peak. (E) SEM image of the board-like precursor crystals. (F and G) TEM images of the layered transducer material NC@Cu<sub>x</sub>O after a short period of pyrolysis under air atmosphere.

To ascertain that copper atoms were highly dispersed at the initial precursor stage, powder X-ray diffraction (PXRD) was performed immediately after lyophilization (Supplementary methods). All of the main peaks have been indexed as a well-defined orthorhombic phase of *trans*-[Cu(NO<sub>3</sub>)<sub>2</sub>(Him)<sub>4</sub>]

crystal (PDF 27-1527)<sup>23</sup>, indicating that the copper ions were strictly hexa-coordinated by four nitrogen atoms (from imidazole) and two oxygen atoms (belonging to the nitrate ions) (Fig. 1B). The specific crystal herein was obtained according to the following procedures: N,N'-carbonyldiimidazole (CDI) underwent decomposition in some polar solvents like ethanol, thus, releasing free imidazole (Him) molecules as well as di-esters of carbonic acid or imidazole-N-carboxylic esters, as shown in *eq. 1*. Whereas, in the presence of lattice water, CDI was possible to be hydrolyzed into carbonate ions (*eq. 2*) which would further react with copper ions and generate stable basic modalities<sup>24</sup>.



In order to know the priority of the aforementioned possible reaction routes, two contrast synthesis strategies were introduced. In detail, anhydrous copper nitrate with CDI and CuNO<sub>3</sub>·3H<sub>2</sub>O with imidazole were each examined under the same ethanol-solvent condition and compared in terms of their respective diffraction peaks which almost kept the same with a slight peak shift of about 10<sup>-2</sup> degrees, implying lattice shrinkage and bulge of these copper-imidazole frameworks due to the differences in accessory products (Fig. 1C and Fig. S1)<sup>25</sup>. Interestingly, the preferential crystallographic orientations echoed by the diffraction peak intensities, however, were significantly different between the



two groups. From the Fourier transform infrared spectrometer (FT-IR) spectra, it is clear that these Cu-MOFs acquired through different formulas maintained perfectly identical chemical bonds. The transmittance peak variations from the ligand monomers suggested probable reaction routes and the inner connections of MOFs, detailed as follows: 1) the vanishing of carbonyl stretching vibration at  $\sim 1735\text{ cm}^{-1}$ , as well as the strong broad band from 2200 to  $3100\text{ cm}^{-1}$ , respectively indicated the decomposition of CDI, and the following coordination reaction of derived imidazole with copper ion which accompanied the collapse of  $\text{N-H}\cdots\text{N}$  hydrogen bonds; and 2) the strong vibration peak at  $1394\text{ cm}^{-1}$  that can be assigned to the amide C–N of CDI red-shifted to  $1340\text{ cm}^{-1}$  as a result of the formation of ester C–O bonds in all MOF samples (Fig. 1D and Fig. S2)<sup>26</sup>. These results imply that regardless of the presence of lattice water, CDI reacts with ethanol thereby generating ester species.

The bluish violet Cu-MOF powder exhibited tabular hexagon-like morphology with a thickness of hundreds of nanometers in scanning electron microscope (SEM) images (Fig. 1E). After the pyrolysis process under air atmosphere, the resulting  $\text{NC@Cu}_x\text{O}$  catalyst, showed an obviously decreased plane size down to 10-nm scale, according to the transmission electron microscope (TEM) results (Fig. 1F and 1G). Furthermore, the absence of aggregated nanoparticles suggested highly dispersed catalytic sites. To further understand the transformation from a Cu-MOF precursor to a

1  
2  
3  
4 148 copper-based catalyst and its accompanying  $\text{H}_2\text{O}_2$  reduction properties,  
5  
6  
7 149 thermogravimetric-differential scanning calorimetry (TG-DSC) analysis was  
8  
9  
10 150 conducted at a  $5\text{ }^\circ\text{C min}^{-1}$  heating rate (Fig. 2B). A sharp weight loss was  
11  
12 151 noticed from 200 to 240  $^\circ\text{C}$ , accompanied with a clear exothermic peak at  
13  
14 152 226  $^\circ\text{C}$ . Thereafter, three representative temperature points (200, 300 and  
15  
16  
17 153 400  $^\circ\text{C}$ ) were set with their corresponding products named  $\text{NC@Cu}_x\text{O-L}$ ,  
18  
19  
20 154  $\text{NC@Cu}_x\text{O}$  and  $\text{NC@Cu}_x\text{O-H}$  respectively.

21  
22 155 When the Cu-MOF precursor was heated at 200  $^\circ\text{C}$  for 2 hours, the  
23  
24  
25 156 obtained  $\text{NC@Cu}_x\text{O-L}$  still preserved the typical lattice characteristics of  
26  
27 157 *trans*- $[\text{Cu}(\text{NO}_3)_2(\text{Him})_4]$ , and its weight loss can be attributed to the desorption  
28  
29  
30 158 of solvent molecules and the decomposition of thermolabile esters. With a  
31  
32  
33 159 further rise in temperature, broad peaks of graphite and copper oxide  
34  
35  
36 160 appeared in the  $\text{NC@Cu}_x\text{O}$  PXRD spectrum (Fig. 2A). By substituting the  
37  
38 161 measured value of full width at half maximum (FWHM) into the Scherrer  
39  
40  
41 162 equation, the crystallite size of the newly formed copper oxide was calculated  
42  
43 163 to be several nanometers, which was in accordance with the lack of gathered  
44  
45  
46 164 clusters in the TEM image <sup>27</sup>. *Via* calcination at 400  $^\circ\text{C}$ , the derived  
47  
48 165  $\text{NC@Cu}_x\text{O-H}$  showed striking peaks identical to that of  $\text{CuO}$ , owing to the  
49  
50  
51 166 deep substitution of oxygen for the initial coordinated nitrogen through atomic  
52  
53  
54 167 transfer.

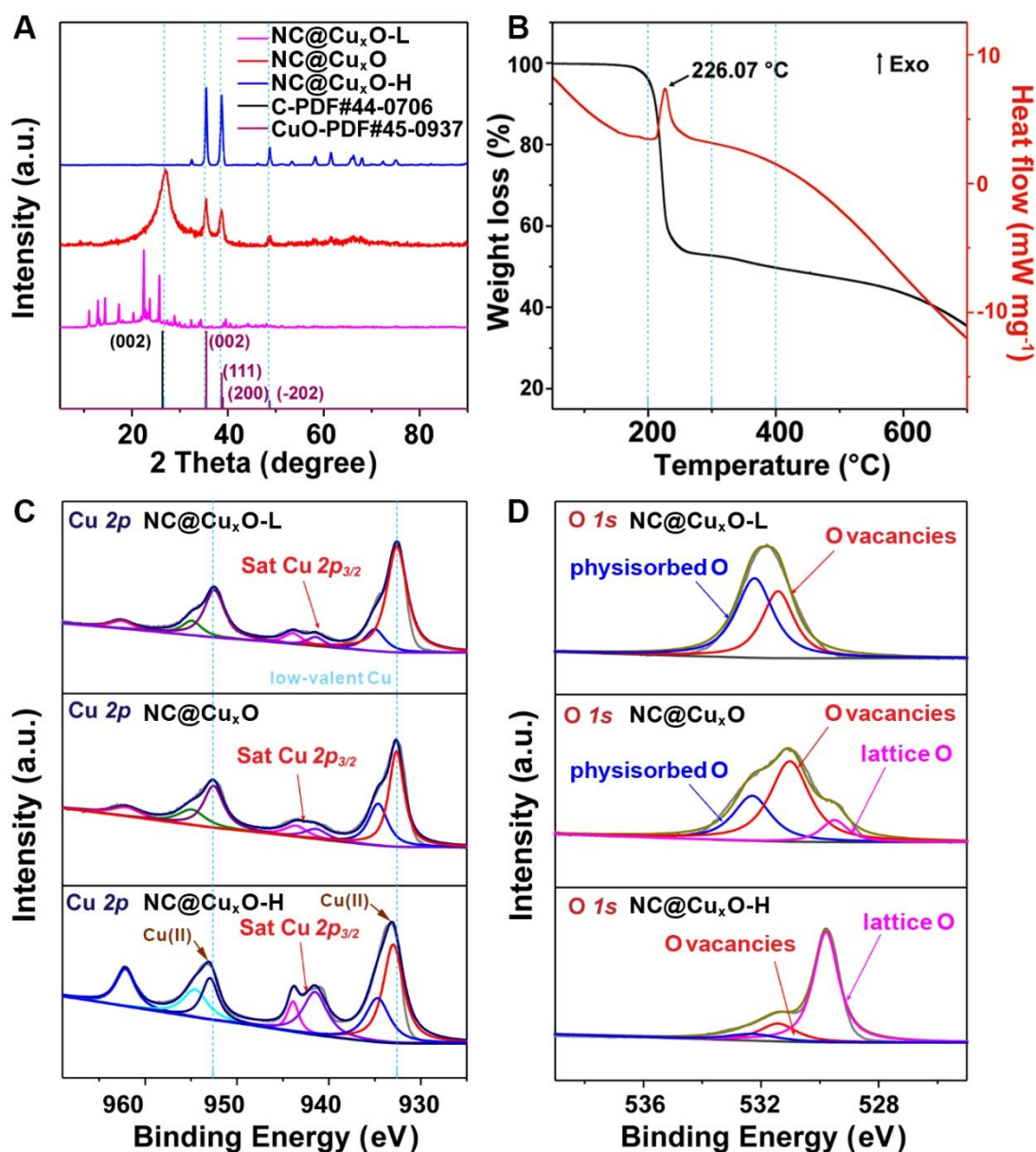


**Fig. 2.** Temperature modulation of the valence state of the central metal as well as the neighboring ligand atoms and vacancies. **(A)** XRD spectra of the pyrolyzed samples under different heat-treatment temperature. **(B)** TG-DSC curves of the self-sacrifice MOF precursor in air atmosphere with the heating rate of 5 °C min<sup>-1</sup>. High-resolution XPS spectra of Cu 2p **(C)** and O 1s **(D)** orbitals of the under-heated NC@Cu<sub>x</sub>O-L, experimental NC@Cu<sub>x</sub>O and over-heated NC@Cu<sub>x</sub>O-H samples.

A mutually corroborating result was obtained by investigating the chemical state alternations of atoms. In both NC@Cu<sub>x</sub>O-L and NC@Cu<sub>x</sub>O samples, the high-resolution X-ray photoelectron spectroscopy (XPS) spectra of Cu 2p orbitals displayed relatively weaker satellite peaks and slightly lower binding

energies of both the  $2p_{1/2}$  and  $2p_{3/2}$  orbitals than that of NC@Cu<sub>x</sub>O-H (Fig. 2C). Due to the existence of CuO nanocrystalline in NC@Cu<sub>x</sub>O, we surmised that these features ought to be attributed to the abundant intermediate low-valent Cu(I) rather than Cu(II) of coordinated state or compound state<sup>28</sup>. Taking O 1s spectra into consideration, on the other dimension, the gradual shift of the predominant sub-peaks from 532.2 to 529.7 eV can help determine the exact components of the aforementioned NC@Cu<sub>x</sub>O catalysts. In detail, NC@Cu<sub>x</sub>O-L displayed Cu-MOF-like characteristics with respect to crystal structure, and the chemical state of organic oxygen assigned as incompletely decomposed esters. NC@Cu<sub>x</sub>O-H, at the other extreme, exhibited canonical CuO properties with a standard XRD pattern and typical XPS spectrum features, such as the intensive satellite peaks of Cu 2p and the nearly complete conversion to lattice oxygen which belongs to the metal-oxide compounds (Fig. 2D).

The aforementioned under- or over- heating treatments exhibit variance in the resulting functional ingredient of the composite catalyst NC@Cu<sub>x</sub>O. On one hand, the crystalline framework collapsed and recombined as a N-doped carbon substrate. The copper atoms, on the other hand, were gradually aggregated and oxidized into nanoscale CuO nanoparticles, while preserving an overall amorphous state with abundant oxygen vacancies (Fig. 2D)<sup>29</sup>. Therefore, the uniformly dispersed catalytic centers of reductive copper oxide in NC@Cu<sub>x</sub>O determined their high reaction activity towards oxidizing

substances. Simultaneously, the internal structural porosity is substantially retained which guarantees sufficient mass transfer during the catalyzing procedures (Fig. S3 and S4). The Cu-MOF precursor's periodic atom distributions and definite melting point enable the investigation of some critical catalyst-evolving processes, such as metal migration and oxygen transfer, by simply modulating temperature.

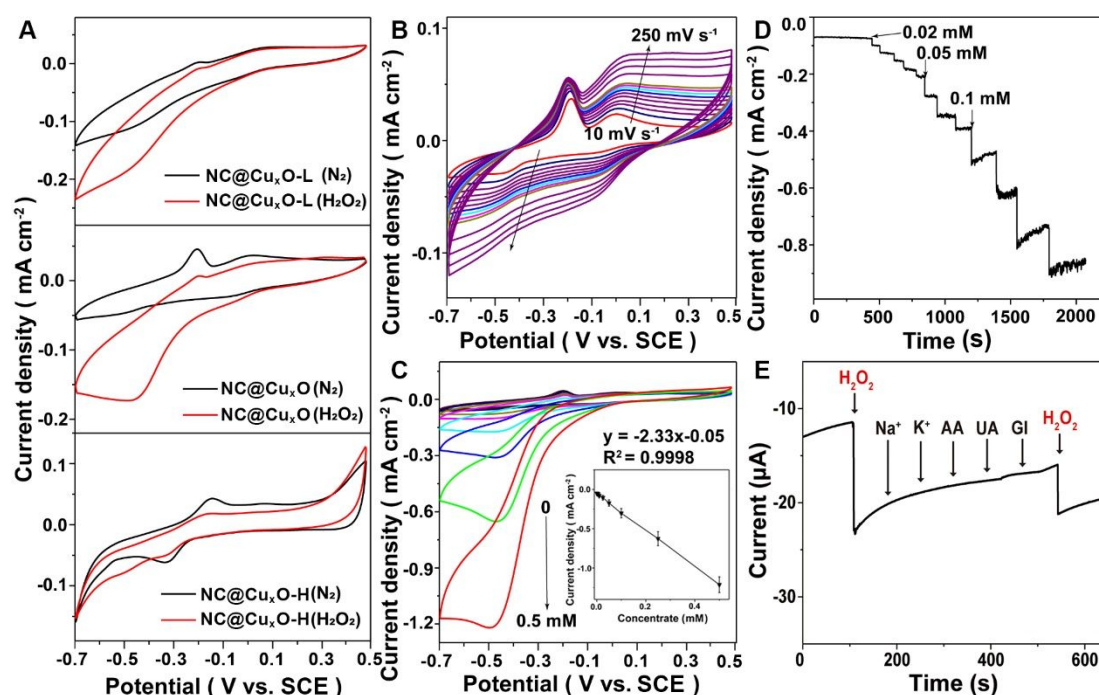


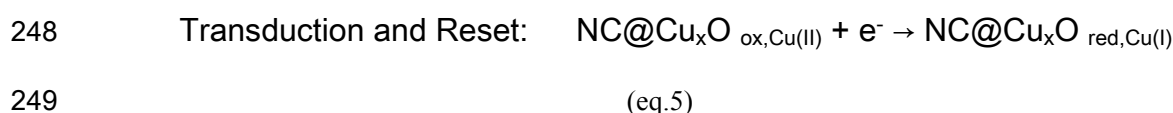
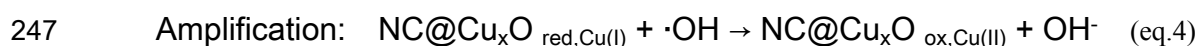
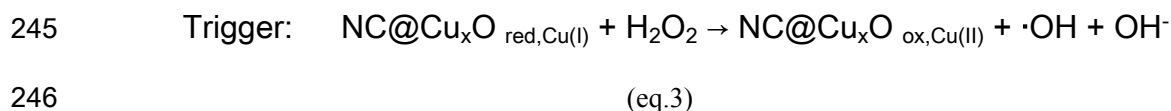
**Fig. 3.** Electrochemical catalysis behavior investigation of the transducer material to support sensitive sensing of H<sub>2</sub>O<sub>2</sub> concentration. **(A)** Electrochemical redox characteristics of the MOF-residual dominant (NC@Cu<sub>x</sub>O-L, top), O-vacancy abundant (NC@Cu<sub>x</sub>O, middle) and deeply oxidized (NC@Cu<sub>x</sub>O-H, bottom) samples as transducers in the absence and presence of 0.05 mM H<sub>2</sub>O<sub>2</sub>. **(B)** Cyclic voltammograms of NC@Cu<sub>x</sub>O electrode at different scan rates from 10 to 250 mV s<sup>-1</sup> in condition of saturated nitrogen without H<sub>2</sub>O<sub>2</sub>. **(C)** Cyclic voltammogram of NC@Cu<sub>x</sub>O electrode in response to H<sub>2</sub>O<sub>2</sub> concentrations of 0 to 0.5 mM with an insert exhibiting the linear fitting of the reductive peak-current density values. **(D)** Chronoamperometric responses of NC@Cu<sub>x</sub>O to stepwise addition of H<sub>2</sub>O<sub>2</sub> at -0.5 V (vs. SCE). **(E)** Selectivity test of the biosensor against some common interferences in body fluid, including 1 mM Na<sup>+</sup>, K<sup>+</sup>, ascorbic acid, uric acid and glucose.

Based on the characteristics of the NC@Cu<sub>x</sub>O catalyst species, their respective electrochemical behaviors were further examined using cyclic

1  
2  
3  
4 221 voltammetry (CV) (Fig. 3A). In the absence of  $\text{H}_2\text{O}_2$ , the lower-heated sample  
5  
6 222 showed inconspicuous redox peaks, implying an inert electron transfer ability  
7  
8  
9 223 of the Cu-N coordinate-bond dominated MOF material. In contrast, the 400 °C  
10  
11 224 pyrolyzed product exhibited both obvious redox peaks ( $\text{Cu}^{\text{I}}/\text{Cu}^{\text{II}}$ ,  $E_p = -0.34$  and  
12  
13  
14 225  $-0.15$  V) due to the formation of conductive carbon substrates. In regard to the  
15  
16  
17 226 NC@Cu<sub>x</sub>O, its undiscovered reduction peak at this particular potential window  
18  
19 227 indicated that copper existed in a low valence state in Cu<sub>x</sub>O and the  
20  
21  
22 228 electrochemically oxidized copper ions would then be released into the liquid  
23  
24  
25 229 phase, resulting in an irreversible procedure. When the solution contained  
26  
27 230 0.05 mM  $\text{H}_2\text{O}_2$ , a strong reduction peak appeared around  $-0.45$  V, significantly  
28  
29  
30 231 deviating from the CV curve without adding  $\text{H}_2\text{O}_2$ . It is worth noting that the  
31  
32  
33 232 oxidization peak, in the meanwhile, became quite indistinct especially when  
34  
35 233 the  $\text{H}_2\text{O}_2$  concentration increased. This result implied that reductive copper in  
36  
37  
38 234 NC@Cu<sub>x</sub>O preferred to react with the oxidizing substances derived from  $\text{H}_2\text{O}_2$   
39  
40 235 decomposition, prior to being electrochemically oxidized at the anode (*eq. 3*).

41  
42  
43 236 The emphasis in sensitive  $\text{H}_2\text{O}_2$  detection lays on enhanced signal  
44  
45  
46 237 transduction or an amplified feedback. Therefore, the catalysis mechanism  
47  
48 238 and its signal conversion process was studied first. The NC@Cu<sub>x</sub>O modified  
49  
50  
51 239 glassy carbon electrode (GCE) was tested by cyclic voltammetry at different  
52  
53  
54 240 scan rates in 0.1 M PBS and 0.3 M KCl solution (Fig. 3B). With increasing  
55  
56 241 scan rate from 10 to 250  $\text{mV s}^{-1}$ , both of the anodic and cathodic peak  
57  
58  
59 242 currents were measured as linear with the square root of the scan rate (Fig.

S5), indicating characteristic diffusion-controlled electrochemical redox behaviors<sup>30</sup> from which we inferred a Fenton-induced enhancing mechanism:



The highly dispersed Cu(I) catalysis centers of Cu<sub>x</sub>O efficiently accelerated the decomposition of H<sub>2</sub>O<sub>2</sub>, while releasing an equivalent amount of ·OH radicals. Thereafter, increased reductive copper sites would be oxidized through rapid radical reactions. At the reduction potential, the newly generated Cu(II) would then get reduced by capturing the electrons from the outer circuit. More importantly, the electrochemical procedures at the electrodes were shown to be rapid, which meant this redox cycle (*eq.3-5*) would continuously proceed until the diffusion limit and simultaneously provide amplified current response<sup>31</sup>. In addition, this catalytic process relied on not only the valence state of copper centers, but also the structural configuration of ligand atoms and defects, which can be supposed from the poor activity of both the NC@Cu<sub>x</sub>O-L and NC@Cu<sub>x</sub>O-H samples.

By adding H<sub>2</sub>O<sub>2</sub> solutions of differing concentrations (Fig. 3C), the current intensity of the reduction peak at -0.45 V was identified as a linear coefficient of the concentration, with a corresponding linear equation:  $j \text{ (mA cm}^{-2}\text{)} =$

265  $-2.33C$  (mM) - 0.05 ( $R^2=0.9998$ ), ranging from 10  $\mu$ M to 0.5 mM. The limit of  
266 detection for the NC@Cu<sub>x</sub>O sensor, (LOD=  $3\sigma/S_d$ , where  $\sigma$  represents the  
267 standard deviation of the current density value measured in blank solution, and  $S_d$   
268 stands for the slope of linear regression calibration line), reached 6.67 nM. Fig. 3D  
269 shows the amperometric response towards concentrated H<sub>2</sub>O<sub>2</sub> solutions. The  
270 cathodic current rapidly achieved steady states and increased in pace with the  
271 addition of H<sub>2</sub>O<sub>2</sub>. The selectivity and stability of this proof-of-principle  
272 biosensor were also evaluated as these two important parameters could  
273 reflect whether an artificial catalyst could mimic or even surpass natural  
274 enzymes in practical use. From Fig. 3E, we can conclude that NC@Cu<sub>x</sub>O has  
275 good selectivity towards H<sub>2</sub>O<sub>2</sub>. The i-t curve in Fig. S6 exhibited the stability of  
276 this electrochemical sensor for long-term continuous detection. After dropping  
277 in 1 mM H<sub>2</sub>O<sub>2</sub> solution, the output current could keep steady for more than 1 h,  
278 indicating that the NC@Cu<sub>x</sub>O nanocomposite did not leach out from the  
279 electrode during multiple cycles of electrochemical redox process, while  
280 maintaining high catalytic activity. By simply modulating the thermal redox  
281 condition of a well-characterized crystalline MOF precursor, both the chemical  
282 valence and coordination environment of the central metal were adjusted to  
283 render a transducer enhanced signal feedback. In comparison with previous  
284 studies which introduced other functional materials or not, this NC@Cu<sub>x</sub>O  
285 electrode offers a highly competitive sensitivity, as well as other decent  
286 performances (Table 1).



1  
2  
3  
4  
5  
6  
7  
8  
9  
10  
11  
12  
13  
14  
15  
16  
17  
18  
19  
20  
21  
22  
23  
24  
25  
26  
27  
28  
29  
30  
31  
32  
33  
34  
35  
36  
37  
38  
39  
40  
41  
42  
43  
44  
45  
46  
47  
48  
49  
50  
51  
52  
53  
54  
55  
56  
57  
58  
59  
60

**Table 1.** Comparison of copper-based electrochemical H<sub>2</sub>O<sub>2</sub> transducer materials on catalysis mechanism and sensitivity performance.

Transducer material	Active-center type	Redox potential (V)	Additional materials	Sensitivity (μA mM <sup>-1</sup> cm <sup>-2</sup> )	LOD (μM)	References
CuO nanoflowers	monoclinic CuO	-0.4 (vs. Ag/AgCl)	n.a.	956.69	0.85	32
Cu <sub>2</sub> O nanoparticles	~100 nm size with (111) facets	-0.42 (vs. Ag/AgCl)	n.a.	28.0	0.2	33
3DIO Au/NiO@CuO	Ni <sup>3+</sup> species	0.5 (vs. Ag/AgCl)	CuO skeleton & AuNPs	650.2	0.0037	34
CuNPs@Y-1,4-NDC-MOF/ERGO	CuNPs supported by ERGO	-0.2 (vs. SCE)	Y-1,4-NDC-MOF & ERGO	8.8	0.43	35
Cu <sub>2</sub> O-rGO-P	cubic Cu <sub>2</sub> O	-0.4 (vs. Ag/AgCl)	rGO paper	77*	3.78	36
NCNT MOF CoCu	Co(0) & Cu(0)	0.5 (vs. Ag/AgCl)	Co(0)	639.5	0.206	37
Cu-Mo <sub>2</sub> C/C	Synergic Mo <sub>2</sub> C with Cu(0)	-0.4 (vs. SCE)	hexagonal β-Mo <sub>2</sub> C	392.7	0.04	38
NC@Cu <sub>x</sub> O	Amorphous Cu <sub>x</sub> O with oxygen vacancies	-0.45 (vs. SCE)	n.a.	2330	0.00667	This work

\* estimated from the offered linear regression curve.

We presented, herein, a sensitive H<sub>2</sub>O<sub>2</sub> sensor constructed with a tailored amorphous Cu<sub>x</sub>O composite catalyst. The corresponding mechanism of enhanced signal transduction were stepwise investigated from the precursor conformation, to its catalytic evolution, up to a final amplified electron cascades. With the initial copper-nitrogen square domains converting into low-valent amorphous copper oxide catalytic centers, the resulting current remarkably increased due to its synergistic enhancement, contributed by both rapid radical and electrochemical reactions. Moreover, the structural property of specific neighboring ligand-atom configuration was proven to be a factor as predominant as the valence state of central metals. From the perspective of material, catalysis and the final sensing application, the way to design and

modulate a proper copper-based transducer was comprehensively explored. We envision that our work would hold the prospect for accurate bio-analyte quantitation and promote the mainstreaming of precision diagnosis and medicine.

## Acknowledgements

The authors greatly acknowledge the financial support from National Natural Science Foundation of China (Grant No. 62001224), Natural Science Foundation of Jiangsu Province (Grant No. BK20190457), “Overseas Academic Partnership Program” of Nanjing University of Technology (2019), and Sino-French international research network “New nanostructured materials and biomaterials for renewable electrical energy sources”

1. Zhao, S.; Zang, G.; Zhang, Y.; Liu, H.; Wang, N.; Cai, S.; Durkan, C.; Xie, G.; Wang, G., Recent advances of electrochemical sensors for detecting and monitoring ROS/RNS. *Biosens. Bioelectron.* **2021**, *179*, 113052.
2. Sehit, E.; Altintas, Z., Significance of nanomaterials in electrochemical glucose sensors: An updated review (2016-2020). *Biosens. Bioelectron.* **2020**, *159*, 112165.
3. Lu, S.-M.; Peng, Y.-Y.; Ying, Y.-L.; Long, Y.-T., Electrochemical Sensing at a Confined Space. *Anal. Chem.* **2020**, *92* (8), 5621-5644.
4. Lawal, A. T., Graphene-based nano composites and their applications. A review. *Biosens. Bioelectron.* **2019**, *141*, 111384.
5. Ji, D.; Zhou, H.; Tong, Y.; Wang, J.; Zhu, M.; Chen, T.; Yuan, A., Facile

- 323 fabrication of MOF-derived octahedral CuO wrapped 3D graphene network as binder-free  
324 anode for high performance lithium-ion batteries. *Chem. Eng. J.* **2017**, *313*, 1623-1632.
- 325 6. Wang, H.-F.; Chen, L.; Pang, H.; Kaskel, S.; Xu, Q., MOF-derived electrocatalysts  
326 for oxygen reduction, oxygen evolution and hydrogen evolution reactions. *Chem. Soc. Rev.*  
327 **2020**, *49*(5), 1414-1448.
- 328 7. Bavykina, A.; Kolobov, N.; Khan, I. S.; Bau, J. A.; Ramirez, A.; Gascon, J.,  
329 Metal-Organic Frameworks in Heterogeneous Catalysis: Recent Progress, New Trends, and  
330 Future Perspectives. *Chem. Rev.* **2020**, *120*(16), 8468-8535.
- 331 8. Yang, Q.; Xu, Q.; Jiang, H.-L., Metal-organic frameworks meet metal nanoparticles:  
332 synergistic effect for enhanced catalysis. *Chem. Soc. Rev.* **2017**, *46*(15), 4774-4808.
- 333 9. Sun, T.; Xu, L.; Wang, D.; Li, Y., Metal organic frameworks derived single atom  
334 catalysts for electrocatalytic energy conversion. *Nano Res.* **2019**, *12*(9), 2067-2080.
- 335 10. Ji, S.; Chen, Y.; Wang, X.; Zhang, Z.; Wang, D.; Li, Y., Chemical Synthesis of  
336 Single Atomic Site Catalysts. *Chem. Rev.* **2020**, *120*(21), 11900-11955.
- 337 11. Bao, J.; Yang, G.; Yoneyama, Y.; Tsubaki, N., Significant Advances in C1 Catalysis:  
338 Highly Efficient Catalysts and Catalytic Reactions. *ACS Catalysis* **2019**, *9*(4), 3026-3053.
- 339 12. Wang, R.; Dong, X. Y.; Du, J.; Zhao, J. Y.; Zang, S. Q., MOF-Derived Bifunctional  
340 Cu<sub>3</sub>P Nanoparticles Coated by a N,P-Codoped Carbon Shell for Hydrogen Evolution and  
341 Oxygen Reduction. *Adv. Mater.* **2018**, *30*(6), 29266417.
- 342 13. Abdel-Mageed, A. M.; Rungtaweeworant, B.; Parlinska-Wojtan, M.; Pei, X.; Yaghi,  
343 O. M.; Behm, R. J., Highly Active and Stable Single-Atom Cu Catalysts Supported by a  
344 Metal-Organic Framework. *J. Am. Chem. Soc.* **2019**, *141*(13), 5201-5210.

- 1  
2  
3  
4 345 14. Xiangyu, L.; Shanshan, G.; Han, L.; Luodan, Y.; Yunhu, H.; Piao, Z.; Weichao,  
5  
6 346 B.; Heliang, Y.; Yu, C.; Jianlin, S., Bioinspired Copper Single-Atom Catalysts for Tumor  
7  
8 347 Parallel Catalytic Therapy. *Adv. Mater.* **2020**, *32* (36), 2002246.  
9  
10  
11 348 15. Subarna, M.; Dipankar, B.; Sikta, C.; Sarita, K.; Amitava, P., Copper Nanocluster  
12  
13 349 (Cu<sub>23</sub> NC)-Based Biomimetic System with Peroxidase Activity. *ACS Sustainable Chem. Eng.*  
14  
15 350 **2020**, *8* (49), 18335-18344.  
16  
17  
18 351 16. Mei-Chen, P.; Yan-Mei, L.; Ya-Qin, C.; Ruo, Y.; Ying, Z., In Situ Controllable  
19  
20 352 Generation of Copper Nanoclusters Confined in a Poly-L-Cysteine Porous Film with Enhanced  
21  
22 353 Electrochemiluminescence for Alkaline Phosphatase Detection. *Anal. Chem.* **2020**, *92* (19),  
23  
24 354 13581-13587.  
25  
26  
27 355 17. Wang, W.; Zhang, Y.; Zhang, J.; Li, G.; Leng, D.; Gao, Y.; Gao, J.; Lu, H.; Li,  
28  
29 356 X., Metal-organic framework-derived Cu<sub>2</sub>O-CuO octahedrons for sensitive and selective  
30  
31 357 detection of ppb-level NO<sub>2</sub> at room temperature. *Sens. Actuators, B* **2021**, *328*, 129045.  
32  
33  
34 358 18. Wang, B.; Luo, Y.; Gao, L.; Liu, B.; Duan, G., High-performance field-effect  
35  
36 359 transistor glucose biosensors based on bimetallic Ni/Cu metal-organic frameworks. *Biosens.*  
37  
38 360 *Bioelectron.* **2021**, *171*, 112736.  
39  
40  
41 361 19. Wang, D.; Zhang, D.; Yang, Y.; Mi, Q.; Zhang, J.; Yu, L., Multifunctional  
42  
43 362 Latex/Polytetrafluoroethylene-Based Triboelectric Nanogenerator for Self-Powered Organ-like  
44  
45 363 MXene/Metal-Organic Framework-Derived CuO Nanohybrid Ammonia Sensor. *ACS Nano*  
46  
47 364 **2021**, *15* (2), 2911-2919.  
48  
49  
50  
51 365 20. Chen, Y.-Z.; Zhang, R.; Jiao, L.; Jiang, H.-L., Metal-organic framework-derived porous  
52  
53 366 materials for catalysis. *Coord. Chem. Rev.* **2018**, *362*, 1-23.  
54  
55  
56  
57  
58  
59  
60

- 367 21. Goud, K. Y.; Reddy, K. K.; Khorshed, A.; Kumar, V. S.; Mishra, R. K.; Oraby, M.;  
368 Ibrahim, A. H.; Kim, H.; Gobi, K. V., Electrochemical diagnostics of infectious viral diseases:  
369 Trends and challenges. *Biosens. Bioelectron.* **2021**, *180*, 113112.
- 370 22. Cesewski, E.; Johnson, B. N., Electrochemical biosensors for pathogen detection.  
371 *Biosens. Bioelectron.* **2020**, *159*, 112214.
- 372 23. Stamatatos, T. C.; Perlepes, S. P.; Raptopoulou, C. P.; Terzis, A.; Patrickios, C. S.;  
373 Tasiopoulos, A. J.; Boudalis, A. K., Alcoholysis/hydrolysis of 1,1'-carbonyldiimidazole as a  
374 means of preparing unprecedented, imidazole-containing one-dimensional coordination  
375 polymers of copper(II). *Dalton Trans.* **2009**, (17), 3354-3362.
- 376 24. Staab, H. A., New Methods of Preparative Organic Chemistry IV. Syntheses Using  
377 Heterocyclic Amides (Azolides). *Angew. Chem., Int. Ed.* **1962**, *1*(7), 351-367.
- 378 25. Yao, M.-S.; Zheng, J.-J.; Wu, A.-Q.; Xu, G.; Nagarkar, S. S.; Zhang, G.;  
379 Tsujimoto, M.; Sakaki, S.; Horike, S.; Otake, K.; Kitagawa, S., A Dual-Ligand Porous  
380 Coordination Polymer Chemiresistor with Modulated Conductivity and Porosity. *Angew.*  
381 *Chem., Int. Ed.* **2020**, *59*(1), 172-176.
- 382 26. Hadrich, A.; Dulong, V.; Rihouey, C.; Labat, B.; Picton, L.; Cerf, D. L., Biomimetic  
383 hydrogel by enzymatic crosslinking of pullulan grafted with ferulic acid. *Carbohydr. Polym.*  
384 **2020**, *250*, 116967.
- 385 27. Abdullah, F. H.; Abu Bakar, N. H. H.; Abu Bakar, M., Comparative study of chemically  
386 synthesized and low temperature bio-inspired Musa acuminata peel extract mediated zinc  
387 oxide nanoparticles for enhanced visible-photocatalytic degradation of organic contaminants  
388 in wastewater treatment. *J. Hazard. Mater.* **2021**, *406*, 124779.

- 389 28. Yang, P.-P.; Zhang, X.-L.; Gao, F.-Y.; Zheng, Y.-R.; Niu, Z.-Z.; Yu, X.; Liu, R.;  
390 Wu, Z.-Z.; Qin, S.; Chi, L.-P.; Duan, Y.; Ma, T.; Zheng, X.-S.; Zhu, J.-F.; Wang,  
391 H.-J.; Gao, M.-R.; Yu, S.-H., Protecting Copper Oxidation State via Intermediate  
392 Confinement for Selective CO<sub>2</sub> Electroreduction to C<sub>2</sub>+ Fuels. *J. Am. Chem. Soc.* **2020**, *142*  
393 (13), 6400-6408.
- 394 29. Xiao, Z.; Huang, Y.-C.; Dong, C.-L.; Xie, C.; Liu, Z.; Du, S.; Chen, W.; Yan, D.;  
395 Tao, L.; Shu, Z.; Zhang, G.; Duan, H.; Wang, Y.; Zou, Y.; Chen, R.; Wang, S.,  
396 Operando Identification of the Dynamic Behavior of Oxygen Vacancy-Rich Co<sub>3</sub>O<sub>4</sub> for Oxygen  
397 Evolution Reaction. *J. Am. Chem. Soc.* **2020**, *142* (28), 12087-12095.
- 398 30. Fang, Y.; Luan, D.; Chen, Y.; Gao, S.; Lou, X. W., Rationally Designed  
399 Three-Layered Cu<sub>2</sub>S@Carbon@MoS<sub>2</sub> Hierarchical Nanoboxes for Efficient Sodium Storage.  
400 *Angew. Chem., Int. Ed.* **2020**, *59* (18), 7178-7183.
- 401 31. Savéant, J.-M., Molecular Catalysis of Electrochemical Reactions. Cyclic Voltammetry of  
402 Systems Approaching Reversibility. *ACS Catalysis* **2018**, *8* (8), 7608-7611.
- 403 32. Ni, Y.; Sun, Z.; Zeng, Z.; Liu, F.; Qin, J., Hydrothermal fabrication of hierarchical  
404 CuO nanoflowers for dual-function amperometric sensing of hydrogen peroxide and glucose.  
405 *New J. Chem.* **2019**, *43* (47), 18629-18636.
- 406 33. Juang, F.-R.; Chern, W.-C., Controlled Synthesis of Cuprous Oxide Nanoparticles with  
407 Different Morphologies for Nonenzymatic Hydrogen Peroxide Sensing Applications. *J.*  
408 *Electrochem. Soc.* **2019**, *166* (4), B200-B204.
- 409 34. Zhou, X.; Xu, L.; Lv, J.; Yang, S.; Zhu, S.; Chen, X.; Sun, X.; Dong, B.; Bai,  
410 X.; Lu, G.; Song, H., Au anchored three-dimensional macroporous NiO@CuO inverse opals

411 for in-situ sensing of hydrogen peroxide secretion from living cells. *Sens. Actuators, B* **2019**,  
412 297, 126729.

413 35. Li, C.; Wu, R.; Zou, J.; Zhang, T.; Zhang, S.; Zhang, Z.; Hu, X.; Yan, Y.; Ling,  
414 X., MNPs@anionic MOFs/ERGO with the size selectivity for the electrochemical  
415 determination of H<sub>2</sub>O<sub>2</sub> released from living cells. *Biosens. Bioelectron.* **2018**, 116, 81-88.

416 36. Cheng, C.; Zhang, C.; Gao, X.; Zhuang, Z.; Du, C.; Chen, W., 3D Network and 2D  
417 Paper of Reduced Graphene Oxide/Cu<sub>2</sub>O Composite for Electrochemical Sensing of  
418 Hydrogen Peroxide. *Anal. Chem.* **2018**, 90 (3), 1983-1991.

419 37. Kim, S. E.; Muthurasu, A., Highly Oriented Nitrogen-doped Carbon Nanotube Integrated  
420 Bimetallic Cobalt Copper Organic Framework for Non-enzymatic Electrochemical Glucose  
421 and Hydrogen Peroxide Sensor. *Electroanalysis* **2021**, 33, 1-14.

422 38. Li, B.; Liu, L.-H.; Zhang, X.-F.; Gao, Y.; Deng, Z.-P.; Huo, L.-H.; Gao, S.,  
423 Echinus-like Cu-Mo<sub>2</sub>C/C yolk-shell composites for ultrasensitive detection of hydrogen  
424 peroxide. *Electrochim. Acta* **2021**, 373, 137908.

425